01 Jan 2006

Statistically Steady Measurements of Rayleigh-Taylor Mixing in a Gas Channel

Malcolm J. Andrews

Arindam Banerjee
Missouri University of Science and Technology

Recommended Citation

M. J. Andrews and A. Banerjee, "Statistically Steady Measurements of Rayleigh-Taylor Mixing in a Gas Channel," *Physics of Fluids*, American Institute of Physics (AIP), Jan 2006.
The definitive version is available at https://doi.org/10.1063/1.2185687

Statistically steady measurements of Rayleigh-Taylor mixing in a gas channel

Arindam Banerjee and Malcolm J. Andrews[a)]
Department of Mechanical Engineering, Texas A&M University, College Station, Texas 77843

(Received 2 June 2005; accepted 26 January 2006; published online 28 March 2006)

A novel gas channel experiment is described to study the development of high Atwood number Rayleigh-Taylor mixing. Two gas streams, one containing air and the other containing a helium-air mixture, flow parallel to each other separated by a thin splitter plate. The streams meet at the end of a splitter plate leading to the formation of an unstable interface and of buoyancy driven mixing. This buoyancy driven mixing experiment allows for long data collection times, has short transients, and is statistically steady. The facility was designed to be capable of large Atwood number studies ($A_t \sim 0.75$). We describe initial validation work to measure the self similar evolution of mixing at density differences ($0.035 < A_t < 0.1$). The purpose of this paper is to describe the new high Atwood number gas channel facility and present validation results for experimental runs at Atwood numbers up to 0.1. Diagnostics include a constant temperature hot wire anemometer, and high resolution digital image analysis. The hot-wire probe gives velocity statistics of the mixing layer. A multiposition single-wire technique was used to measure the velocity fluctuations in three mutually perpendicular directions. Analysis of the measured data was used to explain the mixing as it develops to a self-similar regime in this flow. A digital image analysis procedure was used to characterize various properties of the flow and also to validate the hot wire measurements.
 [DOI: 10.1063/1.2185687]

I. INTRODUCTION

Rayleigh-Taylor (R-T) instability is induced when a heavy fluid is placed over a light fluid in a gravitational field. If the planar surface between the two fluids is disturbed with a perturbation of finite amplitude, the disturbances are driven by buoyancy and develop as R-T instability. The interface becomes distorted with time and the wavelengths associated with the initial disturbance interact between themselves causing a mingling process to degenerate into a turbulent mix. Development of the mix was divided by Youngs[1] into three successive regimes. The mix starts with an initial exponential growth of infinitesimal perturbations that correspond with linear stability analysis. At an amplitude about one-half of the wavelength, the instability saturates and the perturbation speed settles at a constant rate. Thereafter, longer wavelengths overtake due to their continuing exponential growth, a phenomenon referred to as "bubble competition." "Once at self-similarity, and with loss of memory of the initial conditions, dimensional analysis suggests that the mixing half-width grows quadratically with time according to the relation, $h \propto gt^2$, where t, is the time and g is the acceleration due to gravity. However, experiments and computations suggest that a more complete description is $h = \alpha(A_t)A_t g t^2$, where the Atwood number, A_t, denotes the governing parameter of the flow defined by $A_t \equiv (\rho_1 - \rho_2)/(\rho_1 + \rho_2)$, ρ_1 and ρ_2 are the densities of air and air-helium mixtures employed in the present work and α a growth rate constant for the flow that is to be determined. For low Atwood numbers (<0.1), the mix is symmetric and α is usually taken as a constant. However, for high Atwood numbers ($\geqslant 0.1$), the mix is not symmetric and would consist of falling spikes and rising bubbles. The values of α would be different with α_{spike} being a function of the Atwood number and α_{bubble} being more or less constant."

R-T instabilities are of interest in industrial applications such as heat exchangers and sprays in internal combustors.[2] They are also of interest in environmental flows such as effluent discharge into rivers and estuaries. R-T instabilities also occur during the implosion phase of the inertial confinement fusion (ICF) process,[3] and in the remnants of a young supernova.[4] There are numerous publications available that report the various aspects of the development of the R-T instability in the linear (early time) regime.[5–8] Recently, there has been significant work on the intermediate and late time evolution of the mixing process.[9–13]

It is a challenging task to study buoyancy driven mixing by placing a heavy fluid over a light one. Read[9] used rockets to accelerate an initially stable stratified mixture downwards. Andrews and Spalding[14] created an unstable buoyancy gradient by quickly inverting a stable stratified mixture. Linden *et al.*[15] began with a heavy fluid over a light fluid, the two fluids being separated by a plate. The plate was withdrawn and buoyancy driven mixing ensued between the two fluids. Snider and Andrews,[10,16] Wilson and Andrews,[17,18] and Ramaprabhu and Andrews[13] used a novel experimental setup in which two streams of fluid (cold water above and hot water below) flow above and parallel to each other separated by a thin splitter plate. The streams meet at the end of a splitter plate creating an unstable interface which leads to buoyancy mixing,[10] albeit at $A_t < 10^{-3}$. Several researchers have under-

[a)]Author to whom correspondence should be addressed. Telephone: (979) 8478843. Electronic mail: mandrews@tamu.edu

taken high A_t measurements of R-T mixing. Cole and Tankin[19] accelerated an initially stable stratified mixture of air and water by using compressed air. However, the experiments were limited by short data collection times of order of milliseconds. Jacobs and Caton[20] accelerated a small volume of water down a vertical tube using air pressure. They used high speed motion picture photography to study 3D R-T instability in a round and square tube with acceleration varying between 5–10 times that of gravity. Kucherenko[21,22] used a drop tank technique that was accelerated using a gas gun to achieve accelerations between $100g$ to $350g$, and an aqueous solution of glycerin and benzene to give Atwood numbers ranging from 0.23 to 0.5. Diagnostics used by Kucherenko involved pulsed x-ray photography. Dimonte[23] studied turbulent R-T growth rates over a comprehensive range of Atwood number (0.1304–0.961) with constant acceleration using the linear electric motor (LEM). Diagnostics involved bilevel laser induced fluorescence (LIF) measurements and backlight photography. All these studies had short data capture times and involved complicated facilities. Large statistical data sets necessary for the turbulence model development are not available for $A_t > 0.1$, and it is this deficiency that the present facility is addressing. The purpose of this paper is to describe the new high Atwood number gas channel facility and present validation results for experimental runs at Atwood numbers up to 0.1. In the process we carefully describe our new gas channel facility, its validation and give new statistical data sets for A_t between 0.035 and 0.1. The present paper lays the foundations for future publications that will describe our work to extend the facility Atwood number to its maximum value of 0.75.

II. EXPERIMENTAL PRELIMINARIES

The experimental setup is similar to the water channel of Snider and Andrews.[10] However, in the present setup, two gas streams are employed, one of air and the other of a helium-air mixture. As with the water channel, the two streams flow parallel to each other with the air (heavy) above the air-helium mixture (light), separated by a thin splitter plate. The streams meet at the end of the splitter plate leading to the formation of an unstable interface and of buoyancy driven mixing. This air-helium buoyancy driven mixing experiment allows for long data collection times, short transients, is statistically steady and is capable of large Atwood number studies ($A_t \leqslant 0.75$). The experiment is statistically steady "in time" but not in space as the flow field develops downstream.

Figure 1 shows the experimental setup. The apparatus consists of an inlet and exit plenum connected by a Plexiglas flow channel which serves as the test section. The gas channel is 3.0 m long, 1.2 m wide, and 0.6 m deep. The inlet plenum is divided into two sections. Both sections are connected to separate 250 W brushless blowers (Dayton, Inc.) that draw air from the atmosphere. The flow velocity is controlled by adjusting the opening of the dampers connected to the suction port of the blowers. A maximum flow velocity of 2 m/s (which corresponds to the maximum volume flow rate of the blowers) is available. In addition, a series of high

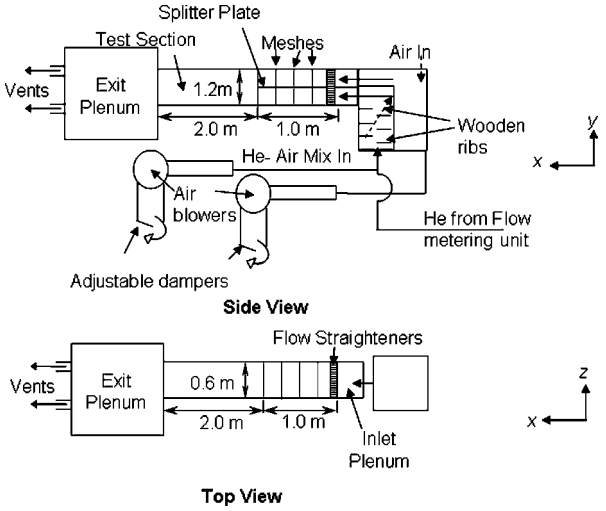

FIG. 1. High Atwood number helium-air gas channel facility used for the experiments.

pressure regulators and an orifice plate meter helium into the lower section of the inlet plenum, helium and air streams are uniformly mixed before they reach the inlet section by passing the streams around a series of wooden ribs placed inside the ductwork (see Fig. 1). A single normal hot-wire probe is placed and various locations at the end of the splitter plate to check whether the mix is uniform. If the mix is not uniform, pockets of helium present in the flow change the heat transfer characteristics of the hot-wire probe leading to a spike in the voltage signal when it flows over the probe. A stainless steel splitter plate extends from the channel entrance to the start of the test section and separates the two streams of gas. The splitter plate is 0.32 cm thick, 1.0 m long, and has a 1.8° knife edge at the end. The test section after the splitter plate is 2.0 m long.

The top and bottom inlet sections of the channel are fitted with screens and flow straighteners to produce a uniform flow, and assist in dissipating free stream turbulence as well as minimizing the boundary layer on the splitter plate and walls.[10,24,25] A 10 cm long flow straightener sits at the entrance of each channel and is made of polycarbonate honeycomb (Model#PCFR250W4.00 Plascore, Inc.), in which each honeycomb cavity is 0.635 cm in diameter. The flow straightener is followed by three screens of 30×30 meshes with a 0.0216 cm wire diameter. A full channel screen is placed at the end of the splitter plate as it is found to be effective in minimizing the wake from the splitter plate.[26] This end screen consists of a 40×40 mesh with a 0.0165 cm wire diameter.

A. Calibration of mass flow rate

The velocities of the two streams were set so that there is no shear between the flows ($U_{\text{air}} = U_{\text{mixture}} = U_m$). This was ensured by introducing puffs of smoke in both the top and bottom sections of the channel through small holes on bottom and top and checking for shear. When at no shear, since the cross-sectional area (A) of the top and bottom sections was identical, the volumetric flow rate of air and helium-air

mixture in the top and bottom channels, respectively, were equal. The mixture flow rate in the bottom section of the channel was then given by:

$$\dot{V}_{\mathrm{mix}} = \dot{V}_{\mathrm{air}} + \dot{V}_{\mathrm{He}} = \dot{V}_{\mathrm{air}} + \frac{\dot{m}_{\mathrm{He}}}{\rho_{\mathrm{He}}} = U_m A. \tag{1}$$

The density of the air-helium mixture was calculated based on thermodynamic principles and primarily depends on the mass flow rate of helium ($\dot{m}_{\mathrm{He}}$) and the velocity of the two streams (U_m) as:

$$\rho_{\mathrm{mix}} = \rho_{\mathrm{air}} + \frac{\dot{m}_{\mathrm{He}}}{U_m A}\left[1 - \frac{\rho_{\mathrm{air}}}{\rho_{\mathrm{He}}}\right]. \tag{2}$$

The Atwood Number of the mix was hence given by:

$$A_t = \frac{(\rho_{\mathrm{air}} - \rho_{\mathrm{mix}})}{(\rho_{\mathrm{air}} + \rho_{\mathrm{mix}})} = \frac{\left[\frac{\rho_{\mathrm{air}}}{\rho_{\mathrm{He}}} - 1\right]\frac{\dot{m}_{\mathrm{He}}}{U_m A}}{2\rho_{\mathrm{air}} + \left[1 - \frac{\rho_{\mathrm{air}}}{\rho_{\mathrm{He}}}\right]\frac{\dot{m}_{\mathrm{He}}}{U_m A}}. \tag{3}$$

Since the mass flow rate of helium ($\dot{m}_{\mathrm{He}}$) was needed to evaluate the Atwood number in (3), an accurate measurement of the helium mass flow rate was required. Initial consideration was given to using a commercial gas flow meter or controller. However, for the range of pressures (~2000 psig) and mass-flow rates being used (~0.1 lbm/s), such flow meters were expensive and complex. Furthermore, calibration data obtained from the manufacturers were based on air and use of empirical laws to compensate for the effects of helium meant that the flow meters would require recalibration. Thus, it was decided to use a volumetric method at constant outlet pressure for flow metering, in which, the gas was delivered from a supply, having passed through an orifice.[27] The main feature of the current setup was the use of a thin orifice for flow constriction and metering. The pressure drop across the orifice was maintained so that the pressure ratio between the downstream and upstream locations was below the critical pressure ratio. Hence, the flow was choked at the orifice and thus the mass flow rate through it was determined based on empirical relations.[28] To this end, the mass flow rate was measured by placing helium bottle(s) on a sensitive digital readout and recording the change in weight of the bottle with time (the uncertainty of the digital scale was ±0.01 lbs). The measured mass flow rate was compared with the theoretical calculations and a coefficient of discharge was determined for the range of orifices used.

Figure 2 shows a schematic of the setup used for controlling and metering the mass flow rate of helium into the gas channel. Two high pressure regulators $R1$ and $R2$ (TESCOM, Inc.) were used to control the pressure drop from a supply pressure of ~2000 psig to the ambient pressure inside the channel where the unit vents the helium. Two high pressure gauges (Swagelock, Inc.) were connected as shown in the schematic to accurately read the pressure in the line at two different downstream locations to ensure that the flow chokes at the orifice and not at either of the regulators. Flexible $1/2$ in. diameter steel tubing was used to connect all components and an orifice plate was placed after the downstream pressure gauge, and held in position by the flow control valve. Initially, the flow control valve was closed and the pressure regulators were adjusted: the upstream regulator was fixed at 1050 psig to ensure that the pressure ratio across $R1$ exceeds the critical pressure ratio and thus the flow was not choked at $R1$; and the downstream pressure regulator $R2$ was set at 550 psig to ensure the flow was not choked at $R2$. Thus when the flow control valve was opened, the flow was immediately choked at the orifice thus ensuring a constant mass flow rate of helium until the pressure in the bottles dropped below the set pressure (550 psig in this case).

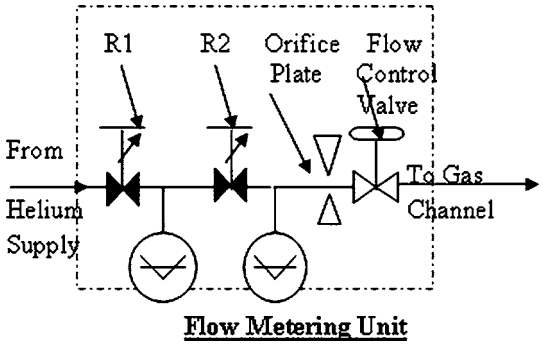

FIG. 2. Constant mass flow rate metering unit for high Atwood number experiments.

Table I shows the results of the mass flow rate calibration for three different orifices of diameters 0.032 in., 0.061 in., and 0.11 in. The theoretical mass flow rate was calculated based on equations for subcritical flow through the orifice.[29] Figure 3 shows the mass flow rates of helium measured at the weighing scale with three different orifices. A straight line fit was performed through the data points obtained and the mass flow rates were tabulated. The R^2 values for the fit in these cases vary between 0.9992 and 0.9998. The Atwood number range given in Table I was calculated based on the experimental mass flow rate. This facility arrangement emptied 90% of the helium tanks at constant mass flow rate. A Kline McClintock uncertainty analysis was performed to calculate the uncertainty in the Atwood number for the experiment. For Atwood numbers of 0.035 and 0.097, the uncertainty in measurement was ±0.002 and ±0.004, respectively, after taking into consideration individual uncertainties of quantities defined in Eq. (4).

TABLE I. Calibrated mass flow rates for different orifices.

Orifice Diameter (in.)	Mass flow rate (lbm/s)		Atwood Number Range
	Experiment	Theory	
0.032	0.0066	0.0072	0.035-0.042
0.061	0.0234	0.0267	0.082-0.100
0.110	0.0796	0.0869	0.194-0.259

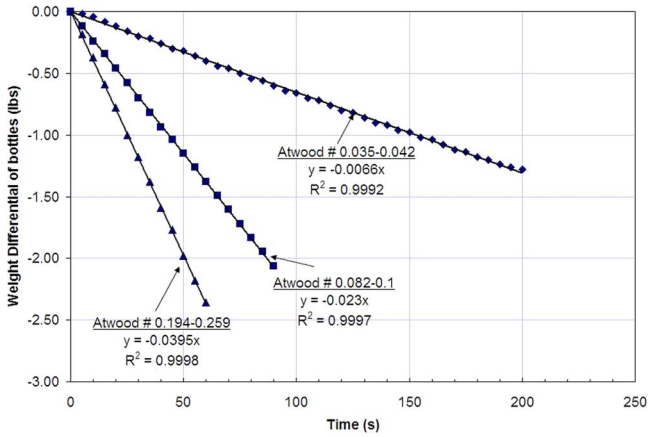

FIG. 3. Calibration of mass flow rate of helium for different Atwood numbers. (Note: For the mass flow rate calibration corresponding to an Atwood No. 0.25, two bottles of helium were used for the calibration. So the actual mass flow rate=2×0.0395=0.0796 lbm/s.)

B. Multiposition measurement technique with the SN hot-wire probe

Velocity measurements were made using a hot-wire probe coupled to a constant temperature anemometer (CTA) unit (Dantec Dynamics). Although our use of CTA is typical, we briefly review its application to measurement of our R-T mix, and note refinements and differences from a typical CTA setup. The CTA unit was an analog instrument designed for measuring velocity in gases and works on the basis of convective heat transfer from a heated sensor to the surrounding fluid, the heat transfer being primarily related to the fluid velocity. The CTA was suited for measurement of fast gas velocity fluctuations of fine scales and high frequencies.[30] The complete measuring system used in the present study consists of (a) a single normal hot-wire probe (SN probe: 55P16) with support and a 4 m BNC-BNC probe cable, (b) mini-CTA anemometer (54T30) with built-in signal conditioner and power adapter, (c) SC 2040 sample and hold board (National Instruments) connected to a PCI-MIO-16E-4 A/D board (National Instruments) mounted in a Pentium 4 computer. NI-DAQ driver software and Lab-View DAQ Software were used for data collection at desired frequencies.

The CTA circuit operates on a bridge ratio of 1:20 and has a frequency response of 10 kHz (3 dB limit). Various CTA and probe parameters are listed in Table II and a 55P16 single normal probe was used in the present measurements. Various parameters given in Table II correspond to specifications for the SN probe (Dantec Dynamics), wherein the overheat ratio determines the working temperature (T_w) of the sensor. An overheat adjustment may be based on either the wire resistance at 20 °C or the measured wire resistance at the actual temperature. A calibration was performed to establish the relation between CTA output and flow velocity by exposing the probe to a set of known velocities, U, and then recording the voltages, E. A curve fit through the points (E,U) gave the transfer function for converting data records from voltages into velocities. Calibration may either be carried out in a dedicated probe calibrator or in a wind tunnel

TABLE II. Operating parameters for mini-CTA.

Probe specific parameters		
Sensor resistance, R_{20}	3.49	Ω
Sensor lead resistance R_L	0.9	Ω
Support resistance, R_s	0.44	Ω
Cable resistance, R_c	0.2	Ω
Sensor TCR, α_{20}	0.0036	/K
Wire operating parameters		
Desired wire temperature T_w	191.43	°C
Operating resistance, R_w	5.64	Ω
Total resistance, R_T	7.18	Ω
Decade resistance, R_D	142.48	Ω
Bridge ratio, M	1:20	
Overheat ratio, a	1.6	

with for example a pitot-static tube as the velocity reference.[31,32] However at low speeds (≤2 m/s), a Pitot tube was found to not be sensitive enough so absolute direct measurement of velocities was needed. For the present study, a separate calibration facility was used as shown in Fig. 4(a). A pressure regulator was used to control the supply from the compressed air line (~100 psig). The air supply was fed to an air proportioner meter (Model # P21A1-BA2, Aalborg Corp.) which could control flow rates up to 60 l/min. A 1 in. diameter PVC pipe was used as the test section. Since the hydrodynamic entrance length is approximately $60d$ (~5 ft), a 10 ft long section of the pipe was used for calibration purposes and the hot wire was inserted [as shown in Fig. 4(a)] towards the rear end so that it was well within the fully developed velocity profile. Corresponding hot wire voltages were obtained in the calibration curve [Fig. 4(b)] for known velocities, and temperature was also recorded during

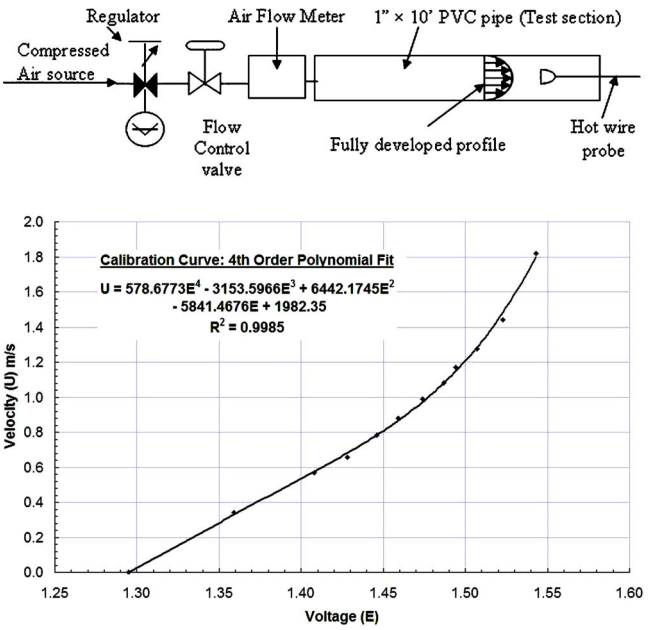

FIG. 4. (a) Schematic of setup used for hot wire calibration. (b) Calibration curve for single normal (SN) probe (55P16) at an overheat ratio of 1.6.

TABLE III. Various measurement orientations for multiposition measurement techniques.

Position	γ	δ
1	0°	0°
2	45°	90°
3	–45°	90°

calibration (T_c). If the mean temperature of the flow (T_a) during the experiment varied from the temperature during calibration, the CTA data records were corrected for temperature variations using Eq. (4)

$$E_{\text{corr}} = \left(\frac{T_w - T_c}{T_w - T_a}\right)^{0.5} \cdot E_a. \tag{4}$$

Calibration of the S-N wire probe was performed over the experimental velocity range of 0–1.8 m/s. A fourth order polynomial plot was fitted to this data and found to have an R^2 value of 0.998. Errors associated with the fourth order fit in Fig. 4(b) can be attributed to errors in velocity measurement inside the gas channel. The maximum error for the range of calibration velocity was less than 1.84%.

For the R-T mix experiments under consideration, velocity fluctuations in all three mutually perpendicular directions were significant. When using a hot-wire probe with a CTA unit, there were two methods by which the velocity fluctuations can be resolved and measured accurately. One method uses a 3-wire probe to resolve all 3 components. However, besides the probe being expensive, this method requires an accurate calibration of the probe. An alternate method, and the one used here, was to resolve the three velocity components using a multiposition single-wire technique,[33] held at different orientations to the flow. The components were not measured simultaneously but by orienting the hot wire (given in Table III) and ensuring that the probe was at the same spatial location. In his analysis, Bruun[33] used a flow that was two-dimensional ($W=0$) with three-dimensional fluctuations. However, since the mean flow field used in the present experiment was one-dimensional ($V=W=0$), the technique of Bruun reduced to three measurements instead of the six roll positions required us to resolve the two-dimensional mean flow. Following Bruun, the velocity vector **V** was taken to have the velocity components $(U+u', v', w')$. Taking into consideration a contribution from the angle of incidence, the equations were resolved to determine the three different orientations as given in Table III. For a wire normal to the mean flow direction, with wire support parallel to the flow (position 1), the mean component U_m, is given by:[33]

$$U_m = U\left[1 + \frac{1}{2}\frac{W^2}{U^2} + \frac{1+2b}{2}\frac{\overline{w'^2}}{U^2} - \frac{W}{U}\frac{\overline{u'w'}}{U^2} - \frac{1+2b}{2}\frac{\overline{u'w'^2}}{U^3}\right]. \tag{5}$$

Since $W \approx 0$ and ignoring third order terms, (5) simplifies to the form for the mean component of the flow as:

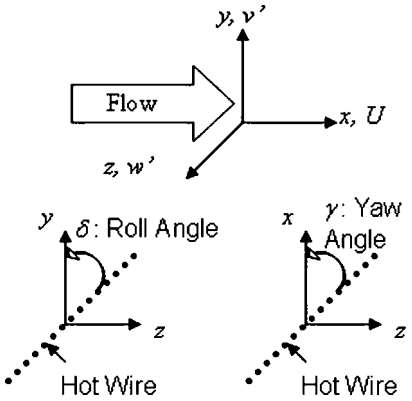

FIG. 5. Coordinate system for measurements and various orientations of hot wire used for measurements (probe axis was normal to the dotted line).

$$U_m = U\left[1 + \frac{1+2b}{2}\frac{\overline{w'^2}}{U^2}\right]. \tag{6}$$

In Eqs. (5) and (6), b was a constant of calibration for the probe and was calculated from the following relation:

$$U_{\pm\gamma} = U(1 + b \cdot \sin^2 \gamma), \tag{7}$$

where $U_{\pm\gamma}, U$ were the velocities measured during calibration in air. The fluctuating component measured by a hot wire placed in position 1 (see Table III and Fig. 5) can be written as:

$$\overline{u_m'^2} = \overline{u'^2}\left[1 + 2\frac{W}{U}\frac{\overline{u'w'}}{\overline{u'^2}} + (1+2b)\frac{\overline{u'w'^2}}{\overline{u'^2}U} - (1+2b)\frac{\overline{u'^2w'^2}}{\overline{u'^2}U^2}\right]. \tag{8}$$

Again, since $W \approx 0$ and ignoring higher order terms, (8) simplifies to:

$$\overline{u_m'^2} = \overline{u'^2}. \tag{9}$$

For a wire yawed to mean flow direction at an angle $\pm\gamma$ (position 2 and 3, see Table III and Fig. 5), the mean component can be expressed as:

$$U_{\pm\gamma} = U(\cos^2\gamma + k^2 \sin^2\gamma)^{1/2}\left[1 + \frac{1+2b+A\tan^2\gamma}{2}\frac{\overline{w'^2}}{U^2} - \frac{1+2b+A\tan^2\gamma}{2}\frac{\overline{u'w'^2}}{U^3}\right], \tag{10}$$

where b was the constant of calibration defined earlier, k the yaw coefficient and, A, a coefficient which accounts for the effect of yaw dependence on measurements,

$$k = \frac{1}{\sin\gamma}\left[\left(\frac{E^2_{\gamma=\pm45°} - E^2_{U=0}}{E^2_{\gamma=0°} - E^2_{U=0}}\right)^{2/0.5} - \cos^2\gamma\right]^{1/2}, \tag{11a}$$

$$A = \frac{\cos^2\alpha \cdot (1-k^2)}{\cos^2\alpha \cdot (1-k^2) + k^2}. \tag{11b}$$

Ignoring third order terms, and simplifying, gives:

$$U_{\pm\gamma} = U(\cos^2\gamma + k^2\sin^2\gamma)^{1/2} \times\left[1 + \frac{1 + 2b + A\tan^2\gamma}{2}\frac{\overline{w'^2}}{U^2}\right]. \quad (12)$$

In addition, the fluctuating component (ignoring third and fourth order terms) can be written as:

$$\overline{u'^2_{\pm\gamma}} = (\cos^2\gamma + k^2\sin^2\gamma)(\overline{u'^2} + A^2\tan^2\gamma\cdot\overline{v'^2} \mp 2A\tan\gamma\cdot\overline{u'v'}). \quad (13)$$

A value for $\overline{v'^2}$ was obtained by adding Eq. (13) to $\gamma = +45°$ and $-45°$ to get

$$\overline{v'^2} = \frac{\overline{u'^2_{+45}} + \overline{u'^2_{-45}} - (1+k^2)\overline{u'^2}}{(1+k^2)A^2}. \quad (14)$$

Thus, using Eqs. (9), (12), and (14), the values of $\overline{u'^2}$, $\overline{v'^2}$, and $\overline{w'^2}$ can be evaluated. The values of k and A were evaluated by performing a yaw calibration for the wire.[31,34]

Errors in hot-wire measurements: Studies conducted by Pierce and Ezekwe[35] and Ezekwe *et al.*[36] reveal that errors involved in the use of a multiposition single wire probe were comparable to an X-wire probe. There were two significant elements in the use of multiposition measurements of turbulent fluctuations. First, the method was based on sequential measurement at different orientations and was sensitive to changes in flow condition. Care was taken to ensure that the mean flow remained constant and the probe was placed at the same location for each successive run. Secondly, since the mean flow field was predominately one-dimensional ($V = W = 0$), the technique of Bruun[33] reduced to three measurements instead of the six roll positions required to resolve a three-dimensional mean flow. This reduced the errors involved in the measurements as the number of positions was cut in half. Swaminathan *et al.*[37] carried out an analysis for parallel probe-stem orientation in a flow field similar to the one used here. They plotted the errors associated with the mean velocity as a function of the turbulence intensity of the flow. Their study shows that if the turbulence intensity of the flow varied between 10%–12%, the maximum error associated with the SN wire measurements would be between 0.5%–1.0%, which was consistent with our observations reported later in Sec. III D. Jørgensen[30] reports a similar range of uncertainties in velocities measured with an identical combination of SN wire probe and mini-CTA setup.

Effect of helium: One concern was measuring velocity fluctuations in a flow involving a binary mixture of helium and air. The hot wire measurements in the current study were at an Atwood number of 0.035, which contains a small volume fraction of helium. It was verified by a careful calibration that the presence of such a small trace of helium does not significantly change the measurements. An extensive literature survey was also conducted to study the response of a hot wire in a flow consisting of a variable concentration of binary gas mixture.[38–43] It was found that various combinations of hot film and hot wire at different orientations and spacing have been used to measure the concentration and velocity fluctuations in binary gas mixtures. Several of these studies were found to cover helium-air mixtures[40,41,43] and the findings were consistent with our observations. Thus the calibration in pure air was considered valid and used for analysis. In addition, the velocity fluctuations measured with the hot wire (Table IV) was found to agree with previous measurements done with PIV.[13] Hot wire measurements for high Atwood studies (0.1–0.75) will involve formulating heat transfer correlations to incorporate the effect of binary air-helium mixture on the hot-wire probe.

TABLE IV. Velocity fluctuations (m/s) measured at Atwood No. 0.035 ($U_m = 0.6$ m/s).

Distance from splitter plate: x (m)	1.0	1.75	1.95
u'	0.0879	0.0724	0.0837
v'	0.1051	0.1286	0.1440
w'	0.0729	0.0709	0.0753
u'/U_m	0.1353	0.1114	0.1287
v'/U_m	0.1617	0.1978	0.2216
v'/u'	1.1951	1.7747	1.7218
α	0.1004	0.0702	0.0706
$\tau = \frac{x}{U_m}\left(\frac{A_t g}{H}\right)^{0.5}$	0.8126	1.4220	1.5845

C. Visualization analysis

The lighter fluid (air and helium mixture) at the bottom was colored with dark green smoke (RC105G, Regin HVAC Products). A row of 35 fluorescent lamps backlit the entire channel test section while matte (frosted) acetate paper (Mister Art.com) served as the white background and helped diffuse the light. Each experiment was photographed using a CANON Powershot A80 digital camera and the size of each image was 1024×768 pixels. The digital camera stored the pictures in JPEG format. Pictures were captured in a burst of continuous capture mode, taking 80 images per minute. The camera settings were manually chosen to eliminate variations between images. During capture the camera was set in monochrome mode with a shutter speed of 1/100 s, aperture F/8.0 and ISO 50. The images were then cropped at the same location using a marker near the exit plenum so that the mix width spanned the entire width of the image. The sized of the cropped image was 681×361 pixels, and the images were processed and analyzed using MATLAB. It was found from a wedge calibration[10] that the concentration of smoke must be kept low to maintain a linear relation between the concentration and measured intensity. Figure 6 shows the calibration performed with a wedge of depth (a) of 22 in., width (b) of 24 in., and height (c) of 6 in. The figure shows that the camera response was linear for a dynamic range over 100 pixel intensity values. For gray scale values less that 80 (lower means darker), it was found the camera response became nonlinear. Thus, care was taken to ensure that the calibrated linear dynamic range from 100 to 200 was used during an experimental run.

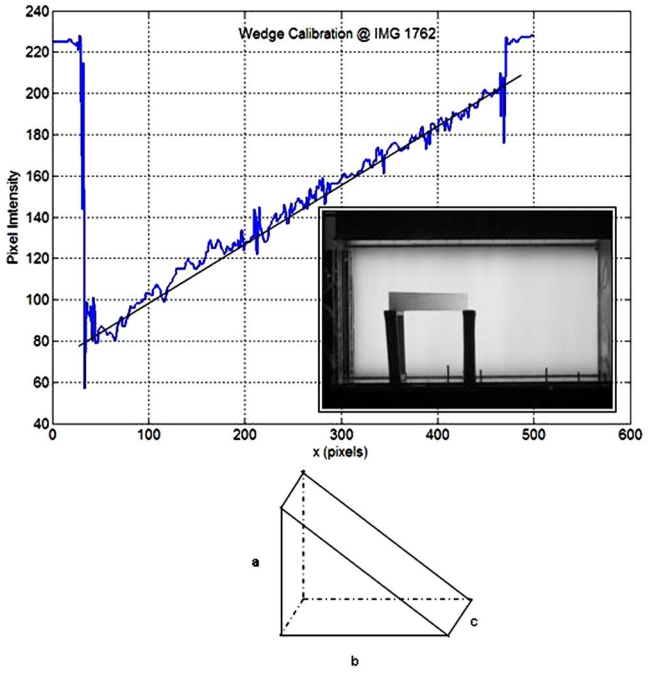

FIG. 6. Intensity as a function of height for calibration wedge (inset shows actual calibration image). [Color wedge dimensions: a (depth)=22 in., b (width)=24 in., c (height)=6 in.]

Extinction of the light from the source I_0 across the path z is given by the Beer Lambert's Law, where κ was the monochromatic extinction coefficient. Expanding the exponential in a series and retaining the first term gives a linear relationship between the applied and transmitted intensities along the path z,

$$I_m(x,y) = I_0 \exp\left(-\int_0^z \kappa dz\right) \approx I_0\left[1 - \int_0^z \kappa dz\right] = I_0(1-\omega), \tag{15}$$

where, $\omega(=\int_0^z \kappa dz)$ was the absolute extinction coefficient of the medium. The extinction coefficient was a function of the volumetric concentration of smoke and the optical path length of light traveled. The calibration (Fig. 6) shows that this approximation was valid from 0% to 60% extinction of the light.

In an ideal experiment, the test section was irradiated with a uniform backlight, and then any two points in the image with the same intensity was a result of an identical attenuation of light. Using a linear relationship between the smoke concentration and intensity, the concentration of the flow field was defined from the intensity distribution. However, the backlight was not uniform, with a light intensity that was bright at the center of the photograph and darker towards the edges. So, a background image was used to correct for nonuniformities in the background intensity to a uniform intensity. The background image was taken from a photograph of the test section without the smoke. The present work used the method of Snider and Andrews[10,44] for correcting the linear intensity to extinction approximation. The corrected measured intensity I_{corr} that would exist if the background intensity was uniform (I_0^{uniform}) can be written as:

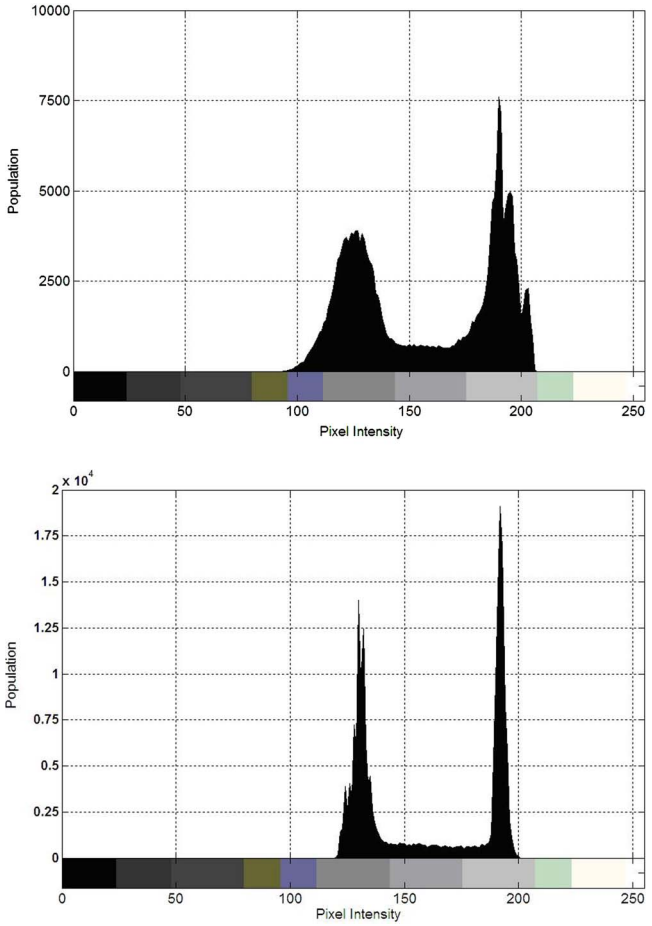

FIG. 7. Histogram for (a) raw image and (b) processed image.

$$I_{\text{corr}} = I_0^{\text{uniform}}(1-\omega). \tag{16}$$

Since ω was a function of the depth of the channel, it can be determined from the measured intensity I_m and the background intensity I_0. Thus eliminating ω between Eqs. (15) and (16) gives:

$$I_{\text{corr}} = \frac{I_0^{\text{uniform}}}{I_0} I_m. \tag{17}$$

The corrected intensity, I_{corr}, was the intensity that would exist if the backlighting were uniform and took in to account the actual background intensity as well as the measured intensity for each pixel. The peak value of a histogram of the background image was selected as I_0^{uniform}. Figures 7(a) and 7(b) show the intensity population before and after adjusting for nonuniform backlighting. In Fig. 7(a), the peaks correspond to regions at the edge or outside the mix, and are thus more prone to nonuniformity in backlighting. The correction for nonuniform backlighting gives narrower peaks for pixel populations at low and high intensities, which correspond to regions where the concentrations were 0% and 100%, and shows improvement obtained with the backlighting correction. These were regions at the periphery of the mix region and the nonuniformity in backlighting was more pronounced in this region.

Errors in visualization: Snider and Andrews[10] reported

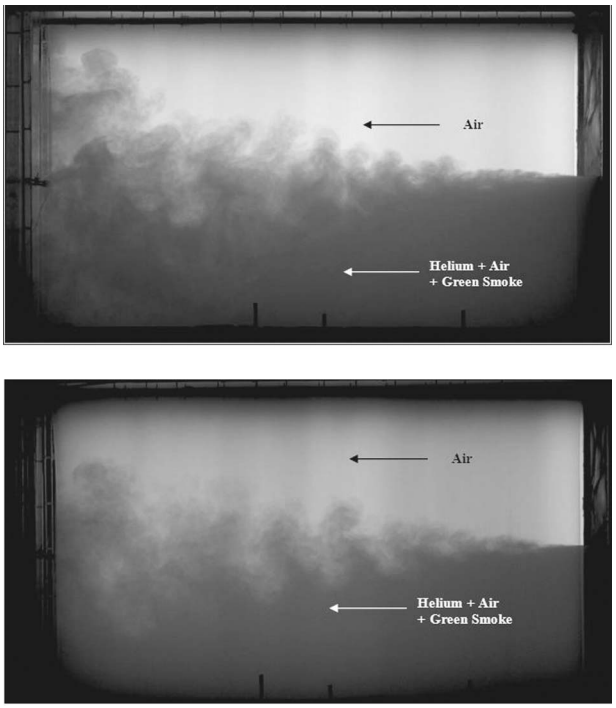

FIG. 8. View of the mixing process in the channel at (a) Atwood No. 0.04 (U_m=50 cm/s) and (b) Atwood No. 0.097 (U_m=85 cm/s).

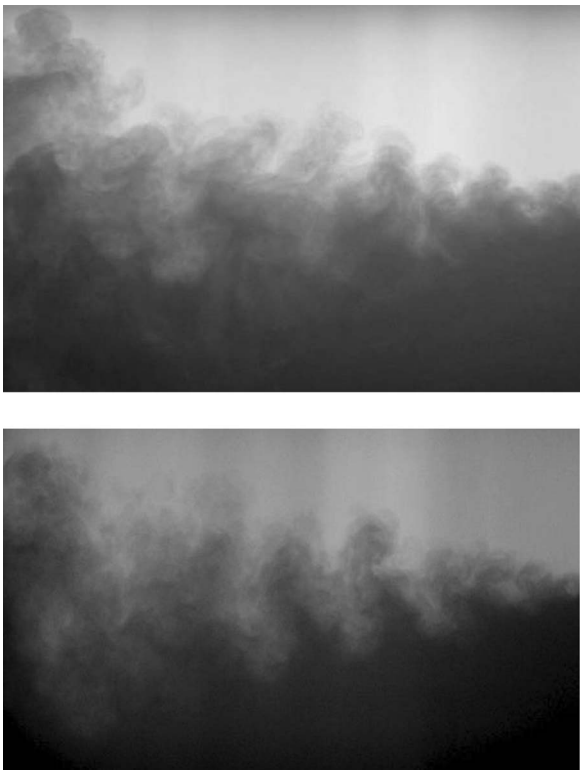

FIG. 9. Close-up view of the three-dimensional plumes across the channel for (a) Atwood No. 0.04 (U_m=50 cm/s) and (b) Atwood No. 0.097 (U_m=85 cm/s).

on the sources of fixed and random errors associated with their dye experiment. Fixed errors such as variations in background lighting were removed by employing the above correction during data analysis. Random errors though often uncontrollable are small in a well designed experiment. The volume fraction f_v, was a random variable determined at each pixel location of an image. Since f_v was a line average through the mixing layer, it was also an estimate of the mean volume fraction, $\overline{f_v}$, which was obtained by averaging over all images. The variance $\overline{f_v}$ was evaluated based on the normalized two-fluid density variance and the total number of volume fraction measurements. The total number of volume fraction measurements was the product of the number of images acquired in a run (400 in the present experiment) and the number of samples in the line average through the mix (361). Through the center of the mix, the line average gave a very large sample because of the relatively large net material flux through the centerline of the mix. The variance in the measured $\overline{f_v}$ close to the centerline was thus negligible.[45] At the edge of the mixing layer where $\overline{f_v}$ was 0.05 or 0.95, the ratio decreases when total number of image ($\sim$400), making the error about $\overline{f_v}\pm 0.025$. This was also evident from the wiggles observed in the fraction profiles at mixture fraction values of 0 and 1, shown in Fig. 10.

III. RESULTS

A. Qualitative observations

Figures 8(a) and 8(b) show photographs of experimental runs at Atwood numbers of 0.04 (U_m=0.5 m/s) and 0.097 (U_m=0.85 m/s). Two gas streams, one containing pure air (top half) and the other consisting of a mixture of air-helium colored with green smoke (bottom half), flow parallel to the splitter plate. The photograph shows the stream mixing and creating an unstable interface driven by buoyancy mixing. As described previously, care was taken to ensure that there was no shear between the two streams. Figures 8 and 9 show a lack of fluctuations or variation of smoke outside the mixing layer, indicating that large scale plumes and small disturbances were confined to the mixing layer. This behavior, which was common in plane shear flow where turbulence was associated with shearing of the streamwise flow,[46,47] was also apparent in the present buoyancy driven flow. The mixing process is one of engulfment of air-helium from below, and air from above, driven by buoyancy, and resulting in a mix region, whose height grows downstream. Figures 9(a) and 9(b), are close up views of the mix, and show that the buoyant mixing layer grows as a front of rising and falling plumes ("bubble and spikes"). Multiple plumes form spanwise across the channel. Vortices form around the edge of the mushroom head of light or heavy fluid as they penetrate through each other. Four major structures were observed at regular frequency along the streamwise direction (right to left). The last two structures in the series (extreme left) were seen to pair. The pictures show that an advanced plume (extreme left) pairs with an earlier plume (second from left). Such "bubble competition" was observed throughout the length of the mix.

B. Mixture fraction measurement

Figures 9(a) and 9(b) show a photograph of the buoyancy driven mixing layer with green smoke introduced in the

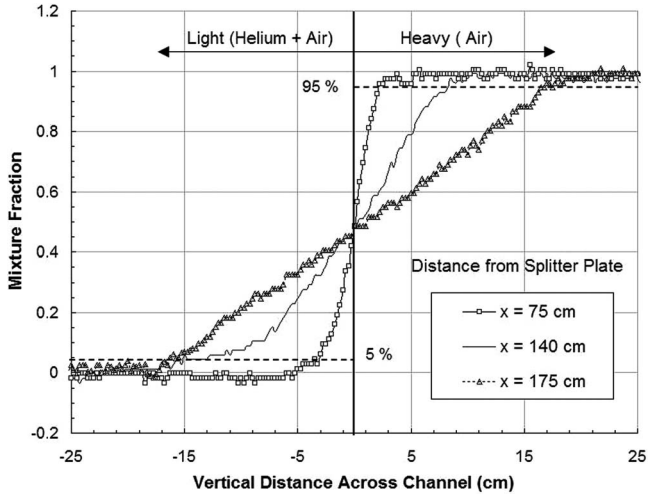

FIG. 10. Mixture fraction distribution across the mixing layer (Atwood No. 0.035).

helium-air mixture. Inspection of the figure reveals that large coherent structures in the light (air) and dark (air-helium-smoke) regions coexist with finer scales of turbulent mixing. The figure also shows that small structures initially form (on the far right) and develop coherently to larger structures downstream (far left). The minimum intensity (dark) corresponds to an air-helium mixture (dyed with green smoke) fraction of zero and the maximum intensity corresponds to a pure air with a mixture fraction of 1. Measured mixture fractions were based on the linear relationship between the dye concentration and pixel intensity as described earlier. In particular, to calculate the fluid mixture fraction, peaks on the corrected image histogram were determined (Fig. 7). These peaks represent the low ($\overline{I_{\min}}$) and the high ($\overline{I_{\max}}$) intensity for the test section and were ensemble averages. Once the minimum and maximum intensities corresponding were established, the fluid mixture fraction was determined from the linear relationship of concentration to intensity as:

$$\overline{f_V}(x,y) = \frac{I(x,y) - \overline{I_{\min}}}{\overline{I_{\max}} - \overline{I_{\min}}}. \tag{18}$$

Figure 10 shows the measured fluid mixture fraction variation at three axial locations of 0.75 m, 1.4 m, and 1.75 m (at three times) taken from images shown from Fig. 8(a). The linear variation of mixture fraction suggests that the air and helium-air mixture were near linearly distributed across the mixing layer in the ensemble average of the turbulent buoyancy driven R-T mixing process. The results compare well with earlier experiments[1,10,11,14] and also with numerical models.[1,48] Figure 11 shows a plot of the 5%, 20%, 50%, 80%, and 95% fraction contours superimposed on the average image (N=400 images). It can be seen that the centerline (50% contour profile) is horizontal across the length of the channel. The 5% and 95% contours show the spread of the mixing layer down the length of the channel.

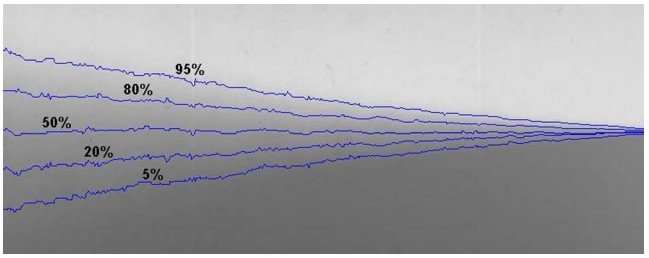

FIG. 11. Contour levels (5%, 20%, 50%, 80%, and 95%) plotted on an average image (N=400) for an experimental run at A_t=0.035 (U_m=0.6 m/s).

C. Mixing width measurement

There are a number of methods to measure the mixing width using a passive scalar. Following Andrews and Spalding,[14] the mix width can be measured as:

$$2h = 6\int_0^H \overline{f_v}(1-\overline{f_v})dy, \tag{19}$$

where the integral can be evaluated from mixture fraction data measured over the width of the channel as in Eq. (19). A factor of 6 comes about by assuming a linear mixture fraction variation through the mixing layer. However, this method does poorly at narrow mixture widths (close to the splitter plate) and was sensitive to noise.[10] A more accurate method to measure the mixing width was to measure the distance between the 0.05 and 0.95 fraction profiles.[14] During an experiment, the velocities were set to let the mix reach the top and bottom walls of the channel close to the exit plenum, thus keeping the mix spread angle below 15° and thus parabolic.[10] The mixture width was measured from ensemble averaged images. The sensitivity to the number of images used on the average was evaluated by comparing mixture widths from 10, 50, 100, and 400 images. Figure 12 shows that the average of 400 images compares well with that from the data of 100 images. It was found that an ensemble average of 100–400 images produced a consistent mixture width measurement.

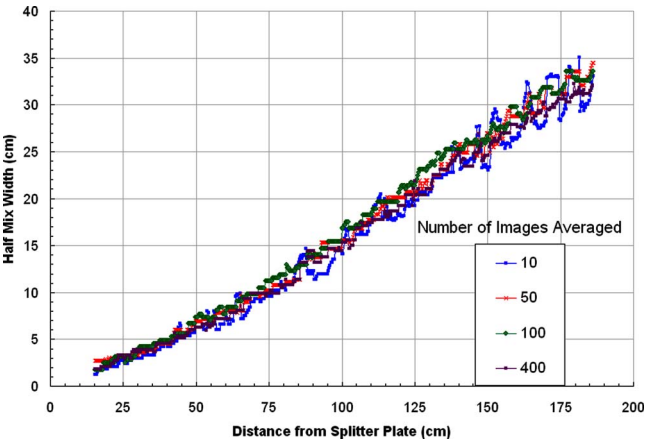

FIG. 12. Effect of number of images on average in the mixing width (Atwood No. 0.035).

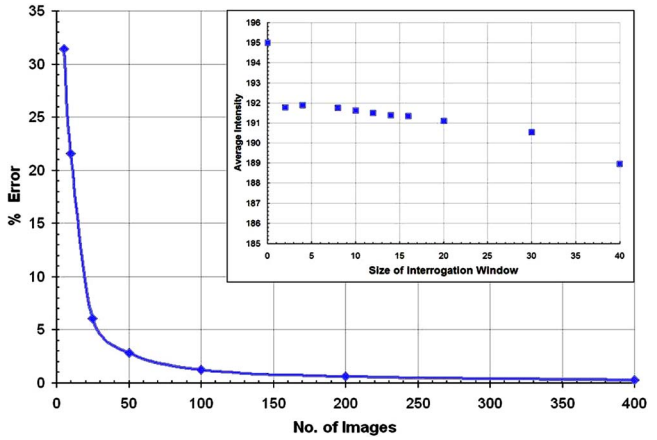

FIG. 13. Percentage (%) rms error as a function of number of images (16×16 interrogation window). [Inset shows average intensity within an interrogation window plotted as a function of the window size (in pixels).]

Uncertainties in density profiles occur due to nonuniform smoke intensity as can be seen near the edge of the mixing layer. To verify that these errors were indeed measurement errors and not as a result of lack of statistical convergence, a detailed statistical convergence test was performed.[49] Assuming that the errors in the mixture fraction (density) measurements were purely random, it was observed that the standard deviation of the density at the edge of the mix falls on a χ^2 distribution.[50] An interrogation window far downstream and close to the edge of the mix was considered. Thus for a given sample size N and a 95% confidence level, the χ^2 distribution was evaluated which gave an estimate of the error in determining density as shown in Fig. 13. The convergence of more than 150 images was also confirmed from the plot of the mix width (Fig. 12). Thus the errors associated with the experimental data from the images were a result of the inherent randomness of the measurement process. The size of the interrogation window also affects the error. An argument similar to the one used in continuum hypothesis was used. A small window would make the local spatial average statistically unreliable as it was based on too few data points. On the other hand, a large window would cause significant flow structures in the field to alter the averages. Thus a plot of intensity versus interrogation window size was plotted at the edge of the mix. It was seen that for a window size of 10–18, the computed averages were not dependent on the size of the interrogation window as it falls in the plateau region in the plot. Thus an interrogation window size of 16×16 was selected for testing of convergence.

The results were compared with a similar analysis performed with PIV images.[49] The current analysis was performed by digital image analysis of the flow section where each image contains information from a number of mix planes along the depth of the channel (image). Thus each image contains information from a number of large structures, both along the direction of flow and also across the depth of the channel. In the current study, the images were captured at a rate of 80 images/min over a 5 min period, so that a large number of large structures were captured in the 400 images used for convergence. In comparison, the PIV image analysis[49] was inherently two-dimensional and the average contained less information. More importantly, the PIV images were captured at a frequency of 30 Hz and a set of 2100 images over a run time of ~70 s. Since the flow speed was significantly less (~5 cm/s), the number of large structures required to obtain statistical convergence was obtained by averaging over 2000 images. Although the statistical convergence in the present study was attained with a lesser number of images, it was concluded that the statistical convergence was a direct consequence of the number of different large 3D structures that were averaged over the duration of the run. So the results are consistent with earlier findings.[49]

D. Measurement of the mix growth parameter (α) analysis from flow visualization

In the far-field (i.e., at a later time), the ensemble averaged half mixing width h is expected to grow as:

$$h = \alpha A_t g t^2 = \alpha A_t g \left(\frac{x}{U_m}\right)^2, \tag{20}$$

where α was expected to be constant at the low Atwood studies performed here. From Fig. 12, it can be seen that although the data follows a near nonlinear trend, the mixing half width does not go to zero at the start of the test section (end of splitter plate). This implies a virtual origin at the start of the splitter plate that accounts for the effect of the splitter plate and the nonsimilarity of the initial mixing layer. Snider and Andrews[10] used an absolute deviation algorithm which defines a virtual origin and fits a linear curve to the mixing half width to evaluate the growth constant. However, this technique was subject to the accuracy of the fitting technique, but was accurate for getting a late-time saturated estimate of α. In the current study, a program was written that determined α based on a "moving window" calculation. This technique used the half-mix width data as discussed earlier in Sec. III. A window with 10 pixels (2.5 cm) contained 10 mixing half widths at each pixel location. The window was used to calculate a slope (dh/dx) for the mixing region by determining a second order polynomial best fit line through the data using a method of least squares. The slope of the best fit line was used to calculate α within the "window." The window stepped along the downstream direction at 1 pixel at a time and calculated α at each location. The slope (dh/dx) was used here as a measure of α to better compare with the value of the growth constant measured from hot wire measurements using the vertical velocity fluctuations v' at the centerline [see Eq. (22)]. Figure 14 shows a plot of α as a function of nondimensional time $\tau[=x/U_m\cdot(A_t g/H)^{0.5}]$, where H is the height of the channel (1.2 m). Inspection of Fig. 14 reveals that α asymptotes to a value of 0.065–0.07 suggesting that the flow reaches self-similarity in this $A_t=0.035$ experiment. Similar observations were recorded in earlier small Atwood ($A_t\sim10^{-3}$) studies.[13]

E. Data from hot-wire measurements

The density gradient needed to create a R-T Instability was obtained by using a heavy fluid (air) over a light one (air-helium mixture). This is different from the low Atwood

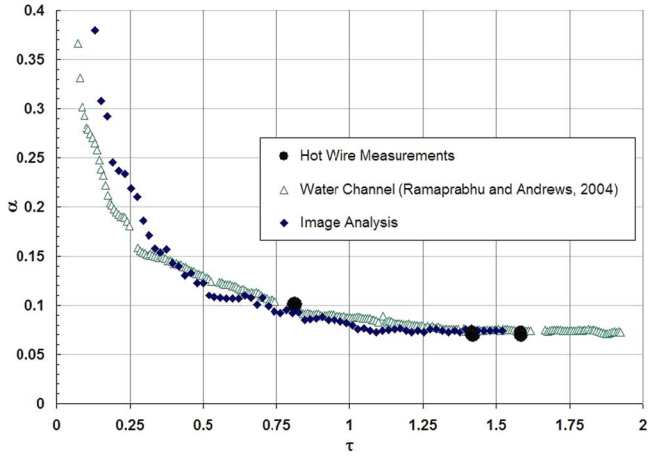

FIG. 14. α at the centerline plotted as a function of τ.

water channel experiments[10] where the instability was created using cold water (heavy) over hot water (light). However, the addition of helium to the mix caused a small temperature gradient ($\sim 2\ ^\circ$C) along the vertical (y) direction (i.e., from the air to the air-helium mixture). We took advantage of this small temperature gradient and used thermocouples to check for the centerline of the mix.[49] The thermocouple temperature diagnostics consisted of an E-type thermocouple (40 gauge wire of nickel-chromium and Constantan) that was positioned at different downstream locations in the channel to ensure that the centerline of the mix remains horizontal.[13,17,18] The thermal response of the E-type thermocouple was ~ 0.001 s deg^{-1} while the uncertainty was $\pm 0.13^\circ$. Initially, the thermocouple was placed close to the centerline of the mixing layer by visual inspection and the data was logged. The centerline offset factor ϕ [as given in Eq. (21)] was computed after the logging process as:

$$\phi = \left[1 + \frac{C_p^{\text{bottom}}}{C_p^{\text{top}}} \frac{\rho_{\text{bottom}}}{\rho_{\text{top}}} \left(\frac{T_{\text{bottom}} - T_i}{T_i - T_{\text{top}}} \right) \right]^{-1}, \tag{21}$$

where C_p^{bottom} and T_{bottom} were the specific heat and temperature of the helium-air mixture (flow at the bottom section of the channel), C_p^{top} and T_{top} were the specific heat and temperature of air (flow at the top section of the channel), and T_i was the temperature of the mix. If $\phi \neq 0.5$, the position of the thermocouple was readjusted using a false positioning method (i.e., linear interpolation) and the data logging process repeated. The thermocouple was adjusted until ϕ approaches a value of 0.5 with an accuracy of 5%.

The hot wire was placed at the prior determined centerline location at various downstream positions from the splitter plate (x=1.0 m, 1.75 m, and 1.95 m). The centerline r.m.s. values of the vertical, v', horizontal, u', and crosswise, w' velocities were determined using the multiposition single wire technique discussed in Sec. II B at τ locations of 0.8126, 1.422, and 1.5845 (for x=1.0 m, 1.75 m, and 1.95 m) from the splitter plate. The results are tabulated in Table IV. Ramaprabhu and Andrews[13] found that the vertical velocity fluctuation (v') at the centerline can be related to the centerline of the mix width by:

$$v' = \frac{dh}{dt} = 2\alpha A_t g t = 2\alpha A_t g \frac{x}{U_m}. \tag{22}$$

Thus, by using (22) and the centerline value of v', we imply that the expansion of the mix was driven by velocity fluctuations that occur across the whole mix and not just the edge. This characterization was also supported by observations of the mixing layer shown in Fig. 8, where large-scale structures span the mix and dominate the velocity fluctuations. Statistics measured in this region remain practically constant across the mix. Thus it is convenient to determine the growth constant α by computing the ratio, $v'/\{2A_t g(x/U_m)\}$. The measured ratio at the three downstream locations is plotted as a function of nondimensional time τ in Fig. 14. It is seen that the results agree with the value of α as found from image analysis by using a moving window technique. Since the Atwood number of 0.035 used for the study is low, it is expected that the dynamics of the R-T mix should be similar to that of the small Atwood number runs in the water channel facility. Thus the growth constant obtained by PIV measurements for a small Atwood run in the water channel is also plotted in Fig. 14. All three sets of measurements of α agree reasonably well, and give a late time value of 0.065–0.07. This consistency across measurement techniques (visualization, PIV, and hot-wire anemometry) and experiments (hot/cold water low Atwood facility, air/helium-air high Atwood facility) demonstrated that the new facility provides consistent statistics for the present experiment ($0.035 < A_t < 0.1$). The saturation of α at late time to a constant value of 0.07 was consistent with the measurements made at the small Atwood water channel facility.[10,13] For low values of Atwood numbers used in the present study, the value of α was expected to be same for both bubbles and spikes (as the structures are symmetric). However for high Atwood numbers ($\geqslant 0.5$), the value of α would be different as the flow will be no longer symmetric but characterized by rising bubbles and falling spikes.[11,23] So for higher Atwood number (>0.1), the formula (22) would not give the same α as that based on mix width measurements, but (22) provides a well defined method for calculating an α based on centerline velocity fluctuations that may be more convenient for validation purposes.

IV. CONCLUSIONS

A statistically steady large Atwood number (0–0.75) experiment has been developed and this paper reports initial experimental runs for low Atwood numbers from 0.035 to 0.1. The experiment allows a heavy fluid to be placed over a light fluid, and a long duration to study the mixing process. Diagnostics used include constant temperature hot-wire anemometer and digital image analysis. A multiposition single-wire technique was used to measure the velocity fluctuations in three mutually perpendicular directions. Analysis of the measured data was used to explain the mixing as it develops to a self-similar regime in this flow and also to provide for a value of the growth parameter (α). A late time value of 0.065–0.07 for α was obtained from the multiposition hot wire technique. A digital image analysis procedure was used

to characterize various properties of the flow and validate the hot wire measurements. The mixture fraction obtained from the visualization analysis suggests that the air and helium-air mixture were linearly distributed across the mixing layer. The value of α obtained by the visualization technique agreed well with that obtained by the hot-wire method. To verify that errors were indeed measurement errors and not as a result of lack of statistical convergence, a detailed convergence test was performed. The study revealed that the statistical convergence was a direct consequence of the number of different large 3D structures that were averaged over the duration of the run.

Measurements of the mixture fraction profiles and the R-T mixing growth rate parameter α for a low Atwood number (0.035) verified the working of the channel when compared with other small and low Atwood experiments by various researchers. We also validated the diagnostics which will be used for future high Atwood number studies. One concern was the effect of helium on the hot-wire measurements. The probe was calibrated in pure air and then used in a flow involving a binary mixture of helium and air. However, since the measurements were made at an Atwood number of 0.035, which contains a small volume fraction of helium (3.5% by volume), the effect of helium on the heat transfer from the probe was negligible and was thus neglected. Future hot wire measurements for high Atwood studies (0.1–0.75) will involve formulating heat transfer correlations to incorporate the effect of binary air-helium mixture on the hot-wire probe.

ACKNOWLEDGMENTS

This material is based upon work that is supported by the U. S. Department of Energy under Contract No. DE-FG03-02NA00060. The authors would also like to thank Wayne Kraft, Nicholas Mueschke, Michael Peart, Gopinath Subramanian, and Michael Martin for their help in construction of the facility.

[1] D. L. Youngs, "Numerical simulation of turbulent mixing by Rayleigh-Taylor instability," Physica D **12**, 32 (1984).
[2] J. C. Beale and R. D. Reitz, "Modeling spray atomization with Kelvin-Helmholtz / Rayleigh-Taylor hybrid model," Atomization Sprays **9**, 623 (1999).
[3] P. D. Roberts, S. J. Rose, P. C. Thompson, and R. J. Wright, "The stability of multiple shell ICF targets," J. Phys. D **13**, 1957 (1980).
[4] S. F. Gull, "The x-ray, optical and radio properties of young supernova remnants," Mon. Not. R. Astron. Soc. **171**, 263 (1975).
[5] G. I. Taylor, "The instability of liquid surfaces when accelerated in a direction perpendicular to their planes I," Proc. R. Soc. London, Ser. A **201**, 192 (1950).
[6] D. J. Lewis, "The instability of liquid surfaces when accelerated in a direction perpendicular to their planes II," Proc. R. Soc. London, Ser. A **202**, 81 (1950).
[7] S. Chandrasekhar, *Hydrodynamic and Hydromagnetic Stability* (Clarendon, Oxford, 1961).
[8] M. Ratafia, "Experimental investigation of Rayleigh-Taylor instability," Phys. Fluids **16**, 1207 (1973).
[9] K. I. Read, "Experimental investigation of turbulent mixing by Rayleigh-Taylor instability," Physica D **12**, 45 (1984).
[10] D. M. Snider and M. J. Andrews, "Rayleigh-Taylor and shear driven mixing with an unstable thermal stratification," Phys. Fluids **6**, 3324 (1994).
[11] G. Dimonte and M. Schneider, "Turbulent Rayleigh-Taylor instability experiments with variable acceleration," Phys. Rev. E **54**, 3740 (1996).
[12] S. B. Dalziel, P. F. Linden, and D. L. Youngs, "Self-similarity and internal structure of turbulence induced by Rayleigh-Taylor instability," J. Fluid Mech. **399**, 1 (1999).
[13] P. Ramaprabhu and M. J. Andrews, "Experimental investigation of Rayleigh—Taylor mixing at small Atwood numbers," J. Fluid Mech. **502**, 233 (2004).
[14] M. J. Andrews and D. B. Spalding, "A simple experiment to investigate two-dimensional mixing by Rayleigh-Taylor instability," Phys. Fluids A **2**, 922 (1990).
[15] P. F. Linden, J. M. Redondo, and C. P. Caulfield, "Molecular mixing in Rayleigh-Taylor instability," in *Advances in Compressible Turbulent Mixing*, edited by W. P. Dannevik, A. C. Buckingham, and C. E. Leith, National Technical Information Service, U.S. Department of Commerce, Springfield, VA. (1992), p. 95.
[16] D. M. Snider and M. J. Andrews, "The simulation of mixing layers driven by compound buoyancy and shear," J. Fluids Eng. **118**, 370 (1996).
[17] P. Wilson, M. J. Andrews, and F. Harlow, "Spectral non-equilibrium in a turbulent mixing layer," Phys. Fluids **11**, 2425 (1999).
[18] P. N. Wilson and M. J. Andrews, "Spectral measurements of Rayleigh-Taylor mixing at small Atwood number," Phys. Fluids **14**, 938 (2002).
[19] R. L. Cole and R. S. Tankin, "Experimental study of Taylor instability," Phys. Fluids **16**, 1810 (1973).
[20] J. W. Jacobs and I. Caton, "Three-dimensional Rayleigh Taylor instability. Part 2. Experiment," J. Fluid Mech. **187**, 353 (1988).
[21] Yu. A. Kucherenko, S. I. Balabin, R. Cherrey, and J. F. Haas, "Experimental investigation into inertial properties of Rayleigh-Taylor turbulence," Laser Part. Beams **15**, 25 (1997).
[22] Yu. A, Kucherenko, S. I. Balabin, R. I. Ardashova, O. E. Kozelkov, A. V. Dulov, and I. A. Romanov, "Experimental study of the influence of the stabilizing properties of transitional layers on the turbulent mixing evolution," Laser Part. Beams **21**, 369 (2003).
[23] G. Dimonte, "Nonlinear evolution of the Rayleigh-Taylor and Richtmyer-Meshkov instabilities," Phys. Plasmas **6**, 2009 (1999).
[24] F. K. Browand and P. D. Weidman, "Large scales in the developing mixing layer," J. Fluid Mech. **76**, 127 (1976).
[25] D. C. Stillinger, M. J. Head, K. N. Helland, and C. W. Van Atta, "A closed loop gravity driven water channel for density stratified flow," J. Fluid Mech. **131**, 73 (1983).
[26] G. K. Koop, "Instability and turbulence in a stratified shear layer," Ph.D. thesis, University of Southern California (1976).
[27] W. Jitschin, U. Weber and H. K. Hartmann, "Convenient primary gas flow meter," Vacuum **46**, 821 (1995).
[28] B. Wu and A. Molinas, "Choked flows through short contractions," J. Hydraul. Eng. **127**, 657 (2001).
[29] J. E. A. John, *Gas Dynamics* (Prentice-Hall, Englewood Cliffs, 1984).
[30] F. E. Jørgensen, "The computer-controlled constant temperature anemometer. Aspects of set-up, probe calibration, data acquisition and data conversion," Meas. Sci. Technol. **7**, 1378 (1996).
[31] G. Buresti and A. Talamelli, "On the error sensitivity of calibration procedures for normal hot-wire probes," Meas. Sci. Technol. **3**, 17 (1992).
[32] S. G. Saddoughi and S. V. Veeravalli, "Hot wire anemometry behavior at very high frequencies," Meas. Sci. Technol. **7**, 1297 (1996).
[33] H. H. Bruun, "Hot-wire corrections in low and high turbulence intensity flows," J. Phys. E **5**, 812 (1972).
[34] H. H. Bruun and C. Tropea, "The calibration of inclined hot-wire probes." J. Phys. E **18**, 405 (1985).
[35] F. J. Pierce and C. I. Ezekwe, "Comparison of Reynolds Stress diagnostics by fixed and rotating probes," AIAA J. **14**, 412 (1976).
[36] C. I. Ezekwe, F. J. Pierce, and J. E. McAllister, "Measured Reynolds stress tensors in a three-dimensional turbulent boundary layer," AIAA J. **16**, 645 (1976).
[37] M. K. Swaminathan, G. W. Rankin, and K. Sridhar, "Evaluation of the basic systems of equation for turbulence measurements using the Monte Carlo technique," J. Fluid Mech. **170**, 1 (1986).
[38] S. Corrisin, "Extended applications of the hot-wire anemometer," NACA-TA 1864 (1949).
[39] Y. Aihara Y., D. R. Kassoy, and P. A. Libby, "Heat transfer from cylinders at low Reynolds numbers. II. Experimental results and comparison with theory," Phys. Fluids **10**, 947 (1967).
[40] R. A. Stanford and P. A. Libby, "Further applications of hot-wire anemometry to turbulence measurements in helium-air mixtures," Phys. Fluids **17**, 1353 (1974).
[41] W. M. Pitts and B. J. McCaffrey, "Response behavior of hot wires and films to flows of different gases," J. Fluid Mech. **169**, 465 (1986).

[42]P. Chassaing, G. Harran, and J. Joly, "Density fluctuations in free turbulent binary mixing," J. Fluid Mech. **279**, 239 (1994).
[43]J. L. Harion, M. F. Marinot, and B. Camano, "An improved method for measuring velocity and concentration by thermo-anemometry in turbulent helium-air mixtures," Exp. Fluids **22**, 174 (1996).
[44]D. M. Snider and M. J. Andrews, "An inexpensive method for quantitative data collection from photographic prints," Meas. Sci. Technol. **6**, 502 (1995).
[45]P. Wilson, "A Study of buoyancy and shear driven turbulence within a closed water channel," Ph.D. dissertation, Texas A&M University (2002).
[46]G. L. Brown and A. Roshko, "On density effects and large structures in turbulent mixing layers," J. Fluid Mech. **64**, 775 (1974).
[47]H. Tennekes and J. Lumley, *A First Course in Turbulence* (MIT Press, Cambridge, MA, 1994).
[48]A. W. Cook and P. E. Dimotakis, "Transition stages of Rayleigh-Taylor instability between miscible fluids." J. Fluid Mech. **443**, 69 (2001).
[49]P. Ramaprabhu and M. J. Andrews, "Simultaneous measurement of velocity and density in buoyancy driven mixing," Exp. Fluids **34**, 98 (2003).
[50]J. Mandel, *The Statistical Analysis of Experimental Data* (Dover, New York, 1964).